ACCSCIENCE PUBLISHING

International Journal of Bioprinting

RESEARCH ARTICLE

Precise tuning of microstructure for surface bacteriostasis using two-photon polymerization 3D printing technology

Fang-Yi Huo[1†], Wentao Zhu[2†], Kan Zhou[3†], Enduo Zhou[1], Lei-Ming Cao[3], Qian Zhu[2], Bo Cai[2*], Lin-Lin Bu[3*], and Hong He[1*]

[1]State Key Laboratory of Oral & Maxillofacial Reconstruction and Regeneration, Key Laboratory of Oral Biomedicine Ministry of Education, Hubei Key Laboratory of Stomatology, Department of Orthodontics, School & Hospital of Stomatology, Wuhan University, Wuhan, Hubei, China

[2]Hubei Key Laboratory of Environmental and Health Effects of Persistent Toxic Substances, School of Environment and Health, Jianghan University, Wuhan, Hubei, China

[3]State Key Laboratory of Oral & Maxillofacial Reconstruction and Regeneration, Key Laboratory of Oral Biomedicine Ministry of Education, Hubei Key Laboratory of Stomatology, Department of Oral & Maxillofacial – Head Neck Oncology, School & Hospital of Stomatology, Wuhan University, Wuhan, Hubei, China

[†]These authors contributed equally to this work.

***Corresponding authors:**
Bo Cai
(bcai@jhun.edu.cn)

Lin-Lin Bu
(lin-lin.bu@whu.edu.cn)

Hong He
(drhehong@whu.edu.cn)

Citation: Huo FY, Zhu W, Zhou K, *et al.* Precise tuning of microstructure for surface bacteriostasis using two-photon polymerization 3D printing technology. *Int J Bioprint.* 2025;11(4):154-164. doi: 10.36922/IJB025150135

Received: April 11, 2025
Revised: May 8, 2025
Accepted: May 19, 2025
Published online: May 19, 2025

Abstract

In nature, many biological surfaces exhibit inherent bacteriostatic property due to the existence of special microstructures. However, the key factors and underlying mechanisms driving this property remain unclear. A significant challenge lies in the lack of proper techniques for precisely fabricating such microstructures as well as finely tuning their morphological parameters. In this study, we adopted a two-photon 3D printing-based approach to fabricate microstructures on specified surfaces with accurate control over their morphology, enabling the investigation of structural bacteriostasis. Through abstracting the subtle morphology on shark skin, we replicated their bacteriostatic microstructures and were able to regulate their morphology at the micron scale. By culturing *Streptococcus mutans* on the surface of these microstructures, we validated their bacteriostatic performance and demonstrated that morphological parameters significantly influenced the efficacy of structural bacteriostasis. Other kinds of microstructures such as micro-holes with bacteriostatic property could also be fabricated and investigated utilizing this two-photon polymerization technology. We believe this strategy offers a powerful tool for researching bacteriostatic mechanisms of various microstructures and will inspire their broad applications in both daily and industrial settings.

Keywords: 3D printing; Antisepsis; Bacteriostatic microstructures; Biomimetics; Two-photon polymerization

1. Introduction

Bacteria have evolutionarily developed robust surface colonization capabilities, allowing them to adhere to a wide range of biological and non-biological surfaces.[1-3] The formation of bacterial biofilms significantly enhances bacterial tolerance to antibiotics,

the host immune system, and other adverse environmental conditions.[4–6] Biofilm-associated infections account for approximately 80% of chronic infections and 50% of nosocomial infections, leading to substantial medical and economic burdens worldwide.[7–9] Anti-bacterial strategies employed across fields such as healthcare, food safety, textiles, and consumer goods comprise physical and chemical approaches. Physical methods, including high temperature/pressure and ultraviolet (UV) radiation, effectively inactivate bacteria but are often limited by material compatibility. Chemical methods, encompassing disinfectants and antibiotics, offer widespread applications but are increasingly challenged by issues like antimicrobial resistance and potential environmental impact.[10–13] Thus, there is an urgent need for innovative approaches to combat bacterial proliferation effectively.

Inspirations for surface bacteriostasis can be derived from nature. Certain biological surfaces, such as cicada wings and lotus leaves, have been shown to possess intrinsic bacteriostatic and anti-wetting properties.[14–16] In the marine environment, biofouling on the surfaces of hard objects has long had a serious impact on shipping, aquaculture, and coastal industries. Its formation originates from biofilms formed by microorganisms and microalgae on the surface of the object in the first place. In order to obtain stable and effective antimicrobial properties, the skin of marine mammals, especially sharks, has been successfully fabricated using bionic replication technology.[17] Interestingly, microstructures imitated from the surfaces of living organisms do exhibit excellent antimicrobial and antifouling properties.[18,19] Additionally, these inherent properties give the material multiple advantages in real-world applications, including extended service life, self-cleaning properties, stability, and avoidance of environmental pollution and safety issues. Therefore, biomimetic antimicrobial materials have become one of the research hotspots in the field of antimicrobial materials that are widely demanded and applied. Gao et al.[20] made membranes with a sea urchin-like texture on the surface by a non-solvent-induced phase separation process and found that such membranes have stronger antimicrobial properties and self-cleaning ability compared to flat membranes. Inspired by the physical antimicrobial form on the surface of insect wings, Li et al.[21] prepared a novel Cu^{2+}-doped nanoarray material on fluorine-doped tin oxide substrate using a one-step hydrothermal method. The surface of this material was uniformly distributed with pyramid-shaped nanoarrays, and the study confirmed that its surface has some physical antibacterial effects against *Staphylococcus aureus* (*S. aureus*) and *Escherichia coli*. The results may be related to the interaction between the morphological effects of the bacteria themselves and the physical structure of the sample surface.

Although various factors affecting the physical inhibitory properties of bionic structures have been reported, such as the type of boundary structure,[22] the type of surface morphology, adherence,[23] and the surface wettability,[24] there is still a large gap in the underlying mechanisms and influencing factors. One of the most notable hindrances lies in the difficulty of precise fabrication and morphology tuning of microstructure with current fabrication methods of chemical synthesis and etching-based techniques.[25–27] Chemical synthesis often requires harsh conditions such as high temperature or high salt environment, while etching-based methods are typically restricted to specific materials such as silicon and glass.[28] More importantly, these fabrication methods face challenges for fine control over individual structural parameters, impeding systematic investigations into the bacteriostatic mechanisms of micro-nano structures.

As an emerging three-dimensional (3D) printing strategy, two-photon polymerization technology enables accurate construction of various 3D topographies on the micron and even submicron scales, providing a powerful tool for research on bacteriostatic micro-nano structures.[29,30] Two-photon polymerization technology was first used for micro- and nano-scale 3D printing in 1965.[31] The near-infrared (NIR) light femtosecond laser acts as a light source to provide sufficient photon flux density to initiate effective polymerization. The resin radical quenching capability and the choice of objective lens determine the resolution of 3D printing, which is now achievable below 100 nm.[32,33] Two-photon polymerization technology can produce nanostructures with very low resolution and arbitrary morphology and has been widely used in cell biology, optical engineering, and medical device development.

In this study, we utilized a strategy based on two-photon polymerization 3D printing technology to precisely regulate the morphological parameters of biomimetic anti-bacterial microstructures, which facilitates our exploration of the key parameters and even the mechanisms behind microstructural bacteriostasis (Figure 1). Specifically, we constructed a shark skin-like bionic microstructure and simplified it to enable us to regulate the morphological parameters of the microstructures. By co-culturing the microstructures with *Streptococcus mutans* (*S. mutans*), we identified their bacteriostatic capacity and confirmed that topographical parameters could significantly affect the bacteriostatic property of the microstructures. Similar results were obtained when we explored the bacteriostatic capacity of other microstructures such as microporous structures. Thus, two-photon polymerization 3D printing

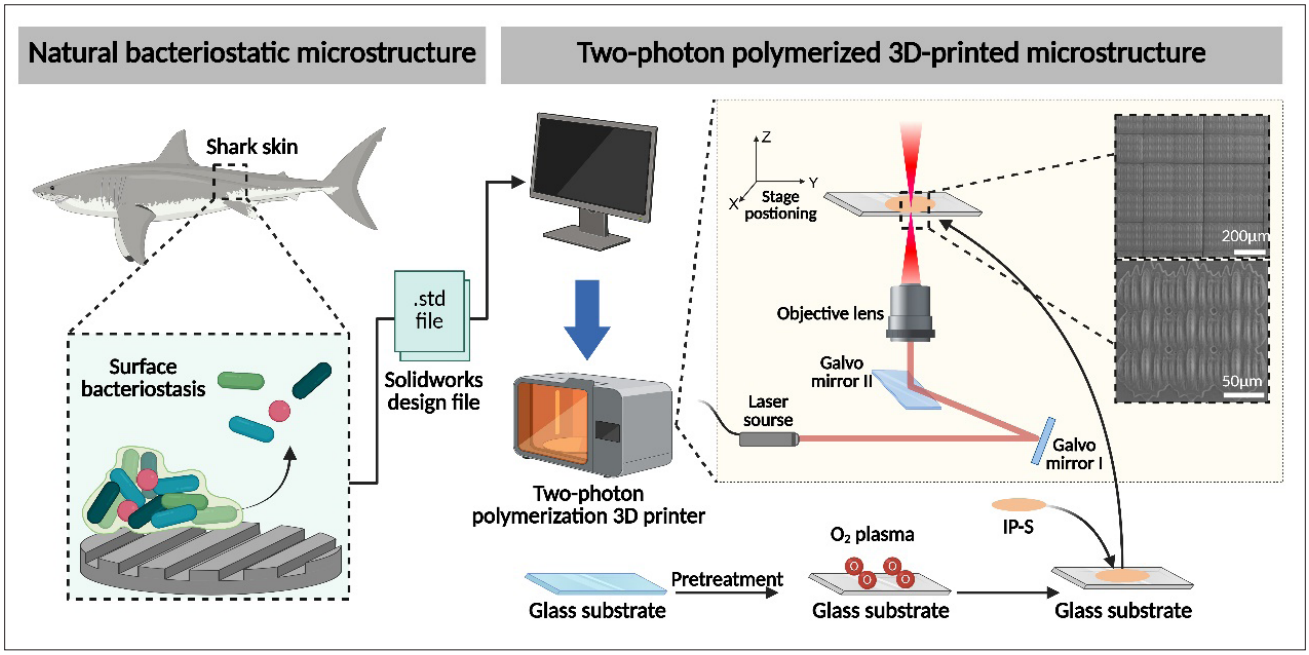

Figure 1. Schematic showing the fabrication of finely tuned bacteriostatic surfaces to inhibit bacterial growth. Bionic microstructures were designed to simulate shark skin using SolidWorks 2019. A photosensitive resin, IP-S, was attached to the substrate surface after pretreatment by oxygen plasma and two-photon polymerization. Finally, the designed bionic bacteriostatic microstructures were accurately constructed on the substrate surface.

technology can be used as a powerful tool to explore the underlying mechanisms and influencing factors of the bacteriostatic capabilities of various microstructures, thereby deepening the understanding of the bacteriostatic mechanisms of micro- and nano-structures and broadening their applications in various aspects of daily life.

2. Materials and methods

2.1. Materials

Photo-sensitive resin (IP-S) and glass substrates were obtained from Nanoscribe, Germany. *S. mutans* was provided by the School & Hospital of Stomatology, Wuhan University, China. Brain-heart infusion (BHI) was obtained from Phygene, China. The reagents of crystal violet and glutaraldehyde were purchased from Sigma-Aldrich, USA. Fluorescent SYTO 9 reagent, phosphate-buffered saline (PBS, 1×, pH = 7.2), and anhydrous ethanol were obtained from Thermo-Fisher Scientific, USA. Agar, propylene glycol monomethyl ether acetone (PGMEA), and isopropanol were purchased from Aladdin, China.

2.2. Design and fabrication of microstructures on glass substrates

The design of the biomimetic microstructures (shark skin denticle simulation and corresponding simplified indented micro-strips) or circular holes microstructure was prepared by SolidWorks 2019 (Dassault Systems – SolidWorks Corporation, USA). Various strips with the same height (3 or 5 μm) and width (2 or 5 μm), yet with different lengths (4, 8, 12, and 16 μm), were arranged in parallel with a 2- or 5-μm-wide gap. Holes with a depth of 3 μm and different diameters (2, 3, and 4 μm) were arranged in parallel, with the spacing between two adjacent holes equal to the hole diameter. The centers of every three adjacent holes formed an equilateral triangle.

For microstructure fabrication, a two-photon laser 3D printer (Photonic Professional GT2, Nanoscribe, Germany) and IP-S were employed. Initially, glass substrates were pre-treated by oxygen plasma (PDC-001, Harrick Plasma, USA) to enhance the affinity between IP-S and the substrates. Subsequently, IP-S was dropped on the glass substrates and placed into the 3D printer for constructing specific microstructures according to design. Finally, PGMEA and isopropanol were employed to develop those microstructures, and PBS was used to wash the substrates to remove excess organic reagents.

2.3. Bacteria cultivation on the surfaces of microstructures

S. mutans was cultured in a BHI solution growth medium and grown at 37°C overnight in static conditions. Substrates with different microstructures were placed into six-well plates and sterilized with ultraviolet (UV) light for 30 min before experiments. Subsequently, *S. mutans* suspension made with BHI broth concentration of 1 × 10^6/mL was inoculated into each well of the six-well

plates to immerse the substrates, which were then left for incubation at 37°C for different periods of time. The substrates were washed gently in PBS three times to remove free bacteria before observation.

2.4. Microscopy and scanning electron microscopy observation

3D-printed microstructures with/without *S. mutans* were observed using a fluorescence microscope equipped with a charge-coupled device (Olympus, Japan). Scanning electron microscopy (SEM; S-3400N, Hitachi, Japan) was employed to further obtain detailed information relating to the microstructures and bacterial proliferation. Substrates with 3D-printed microstructures were sprayed with a thin layer of gold to increase conductivity before SEM imaging. To observe bacteria attached to the microstructures, they were first treated with 2.5% glutaraldehyde solution for 2 h, followed by dehydration using ethanol solutions with different concentrations (30%, 50%, 80%, and 100%, 10 min for each concentration) and complete drying. Then, the microstructures were sprayed with a thin layer of gold for SEM observation.

2.5. Fluorescence staining assays

After incubation with *S. mutans* in BHI solution at 37°C, every substrate with different microstructures was gently washed three times with PBS and then stained by SYTO 9 solution according to the manual from the manufacturer. An inverted fluorescence microscope (NIKON, Japan) was employed to record fluorescent images for bacteria proliferation analysis.

2.6. Statistical analysis

Data were presented as mean ± standard deviation (SD). Unpaired *t*-test or one-way analysis of variance (ANOVA) was used to assess the statistical differences between experimental groups. All the analyses were performed using GraphPad Prism software. A p-value < 0.05 was considered statistically significant.

3. Results

3.1. Two-photon polymerization 3D printing enables construction of biomimetic microstructures and their simplification with bacteriostatic properties

The microstructure of the shark skin surface has been extensively studied for its excellent bacteriostatic properties. Therefore, we first employed the two-photon polymerization-based 3D printing platform (Photonic Professional GT2, Nanoscribe, Germany) to fabricate microstructures inspired by the unique morphology of shark skin.

A drop of IP-S was applied to an oxygen plasma-pretreated glass substrate and processed in the 3D printer to create designed microstructures. As shown in Figure 2a and b, the shark skin denticle simulation was successfully fabricated on the glass substrate. For the feasibility of investigating structural effectiveness, the irregular morphology was abstracted and simplified into a quantifiable, indented micro-strip array with a certain arrangement pattern. The structure that simulates shark skin is characterized by continuous, gentle, longitudinal bulges of varying lengths. The structure of the mimic shark skin is characterized by continuous, gently sloping, and longitudinal rises of varying lengths. We accentuated this feature by simplifying the ridges of the rises into long columns of squares, and the spaces between the ridges were simplified from small slopes to flat surfaces. We then changed the length of the rises from continuously varying to neighboring columns spaced 2 μm apart (ranging from 4 μm increments to 16 μm and then reducing to 4 μm). Finally, this simplified structure featured seven parallel indented micro-strips of varying lengths (4, 8, 12, and 16 μm), with a height of 3 μm, a width of 2 μm, and a spacing of 2 μm, and was fabricated on the glass substrate, as depicted in Figure 2b.

To verify the bacteriostatic efficacy of 3D-printed biomimetic microstructures, *S. mutans*, a representative pathogenic microorganism, was utilized as the model bacterium. The glass substrates, with a 3D-printed flat structure, 3D-printed shark skin denticle simulation, or 3D-printed simplified indented micro-strips, respectively, were co-cultured with *S. mutans* to evaluate bacterial proliferation. In a BHI solution containing 1×10^6 cells/mL, the co-culture of microstructures and *S. mutans* was maintained for 24 h, and bacterial coverage on different surfaces was observed after fluorescent staining and analysis. As shown in Figure 2c, *S. mutans* on the surface with 3D-printed flat structure ("Plane" group) demonstrated vigorous proliferative activity, and their coverage was rapidly expanded. After 8 h of co-cultivation, over half of the surface of the "Plane" group was covered by bacteria. The bacteria continued to proliferate and after 16 h, the "Plane" group was almost entirely covered by bacteria. The rapid proliferation of bacteria serves as a stark reminder, urging us to seek more effective methods of inhibiting their growth.

In contrast, bacterial proliferation on the surface with 3D-printed shark skin denticle simulation ("Simulation" group) was significantly inhibited. After 8 h of co-cultivation, only about 10% of the substrate surface was covered by bacteria, confirming the bacteriostatic properties of the shark skin-inspired microstructure. After 16 and 24 h of co-cultivation, the bacterial coverage in the "Simulation" group gradually increased, but remained substantially lower than in the "Plane" group, at approximately 25% (16 h) and

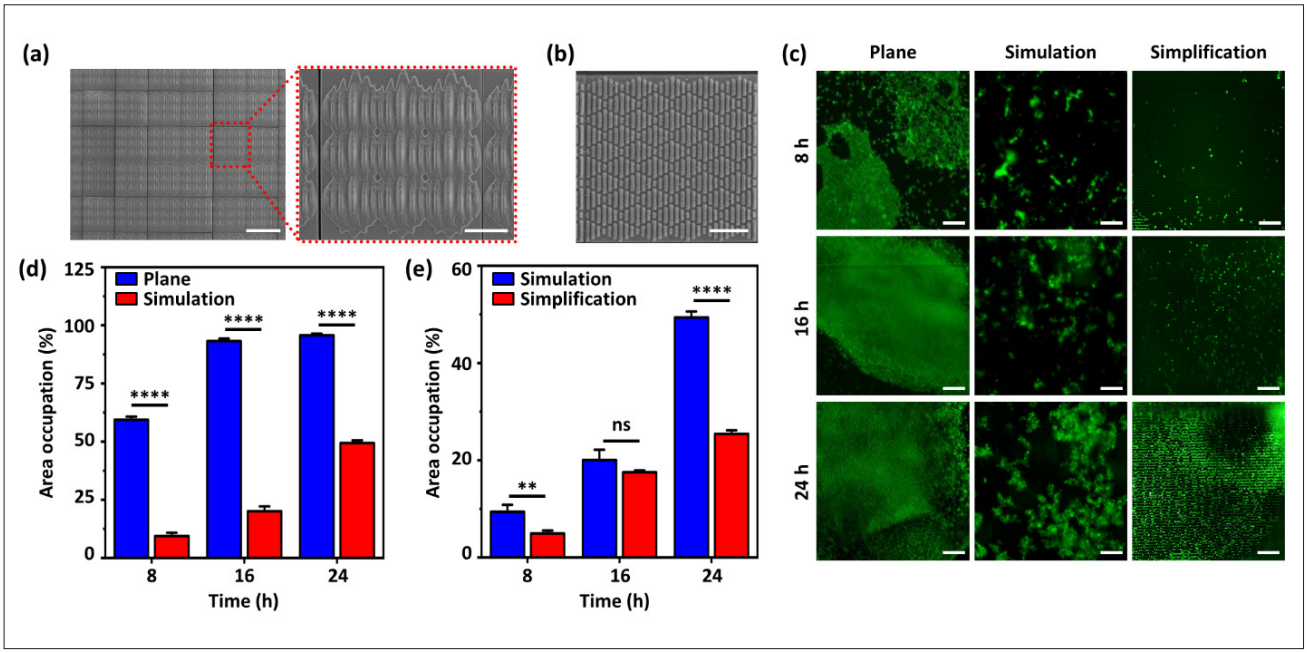

Figure 2. Precisely fabricated shark epidermal structure simulated and simplified microstructure with bacteriostatic ability using two-photon polymerization 3D printing. (a) SEM image of the printed simulated shark skin microstructure. Scale bar: 200 and 50 μm (enlarged). (b) SEM image of the 3D-printed simplified microstructure (the parameters: stripe lengths of 4, 8, and 16 μm; width of 2 μm; height of 3 μm; and distance between stripes of 2 μm). Scale bar: 50 μm. (c) Proliferation of bacteria (green fluorescence-labeled) on flat, shark skin-like microstructures, and simplified microstructures in 24 h. Scale bar: 20 μm. (d) Statistical plot of bacterial proliferation area on the surface with/without printed structures. (e) The simulated and simplified microstructures of shark skin showed significant bacteriostatic effects for at least 24 h. Data are expressed as mean ± SD. n = 3; unpaired t-test; ns, no significance; **p < 0.01; ****p < 0.0001. Abbreviation: SEM, scanning electron microscopy.

50% (24 h), respectively (Figure 2d). The "Simplification" group was obtained by simplifying the microstructure of the sharkskin surface. As shown in Figure 2e, this group exhibited an even lower bacterial coverage after 24 h of co-cultivation compared to the "Simulation" group, indicating that the simplified microstructure possesses superior bacteriostatic properties for at least 24 h. Also, the difference in bacterial proliferation between the "Simplification" and "Simulation" groups implies that the change in microstructural morphology has a significant effect on bacteriostatic properties. Moreover, the simplified structure makes it easier to explore the effect of specific parameter variations on the bacteriostatic properties.

3.2. Influence of different parameters of microstructures on bacterial inhibitory capacity

In order to investigate whether changing the size of the microstructures has an effect on the bacteriostatic effect of the simplified shark skin-like surface microstructures, we utilized two-photon 3D printing to precisely regulate the key parameters of the microstructures, including stripe width (W), height (H), and spacing (S). The standard parameters of the simplified bionic microstructure are as follows: stripe lengths of 4, 8, and 16 μm; W = 2 μm; H = 3 μm; and S = 2 μm (Figure 3a). After 24 h of incubation in BHI solution containing 1 × 10^6/mL *S. mutans*, a limited number of bacteria proliferated on the surface of the simplified 3D-printed bionic microstructures (Figure 3b).

Similarly, we co-cultured *S. mutans* with parameter-adjusted microstructures to specifically evaluate the effect of changing different parameters on the bacterial inhibition performance. On the basis of the standard parameters, we adjusted each of the individual parameters and divided them into three groups: the stripe spacing of "S5" group was adjusted from 2 to 5 μm, the stripe width of "W5" group was adjusted from 2 to 5 μm, and the stripe height of "H5" group was adjusted from 2 to 5 μm. After incubation of different microstructures with *S. mutans* in BHI solution for different periods of time (8, 16, and 24 h), in order to quantitatively analyze the proliferation of *S. mutans*, each substrate of different microstructures was gently washed three times with PBS and then stained with SYTO 9 solution. Fluorescence images were recorded using an inverted fluorescence microscope (Figure 3c). It can be seen that there is a significant difference in the area of the substrate occupied by bacteria proliferating on the surface of the microstructures with different parameters after only 8 h. The area of the substrate occupied by bacteria proliferating on the surface of the microstructures with

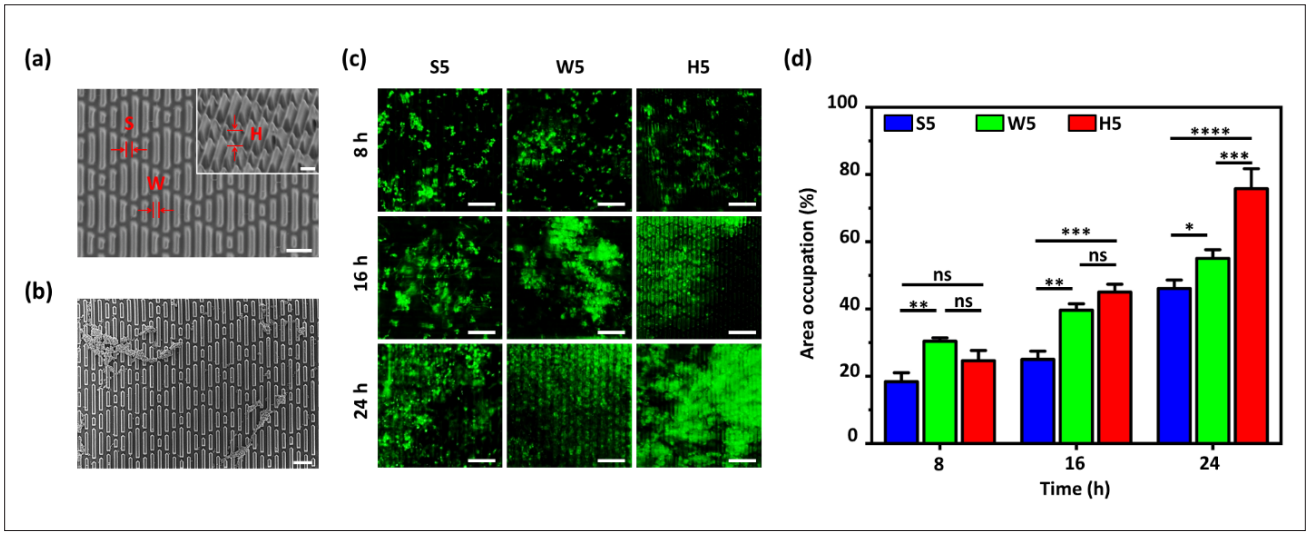

Figure 3. Precise modulation of microstructure morphology using two-photon polymerization 3D printing to investigate the key parameters affecting bacterial inhibition. The standard parameters: stripe lengths of 4, 8, and 16 μm; width (W) of 2 μm; height (H) of 3 μm; and inter-stripe distance (S) of 2 μm. Adjustment of parameters—W: 2–5 μm, H: 2–5 μm, S: 2–5 μm. (a) 3D printing allows precise tuning of microstructural parameters. Scale bar: 10 and 5 μm (inset). (b) SEM image of 3D-printed simplified microstructures with bacterial proliferation on the surface after 24 h. Scale bar: 10 μm. (c) Proliferation of bacteria (green fluorescence-labeled) on printed microstructures with different parameters in 24 h. Scale bar: 30 μm. (d) 24-h proliferation of bacteria on microstructures with different parameters measured in terms of total occupied area on the substrate. Data are expressed as mean ± SD. n = 3; one-way ANOVA; ns, no significance; *p < 0.05; **p < 0.01; ***p < 0.001; ****p < 0.0001. Abbreviation: SEM, scanning electron microscopy.

different parameters was not more than 50% in the "S5" group, but more than 70% in the "H5" group after 24 h. It is hypothesized that the change of a certain parameter of the microstructure has a significant effect on the bacteriostatic function of the microstructure. In addition, the "S5" group was found to maintain the lowest bacterial proliferation at different times compared to the other two groups. It can be hypothesized that there are some specific parameters that can make the physical bacteriostatic capacity of the microstructures the most significant (Figure 3d).

3.3. Bacteriostatic properties of microporous structures alter with structural parameters

In order to explore whether similar structural effects could influence the bacteriostatic capacity, we constructed another microstructure at the micron scale. The surface of this microstructure featured uniformly distributed micropores of the same size, and the diameter of the micropores was used as a parameter adjusted to explore its effect on the bacterial inhibition capacity. To further confirm the effect of parameters on the physical inhibitory capacity, we designed three microporous structures with different pore sizes (pore sizes [*D*] of 2, 3, and 4 μm, respectively) and precisely printed them using two-photon 3D printing technology (Figure 4a). SEM clearly shows bacterial cells proliferated and attached to the 3D-printed microporous structures after 24 h of co-culture with *S. mutans* (Figure 4b). Subsequently, using fluorescent staining and fluorescence microscopy observation records, we compared the substrate area occupied by bacterial proliferation on the surface of microporous structures at different pore sizes. Three groups of microporous substrates with microporous diameters of 2, 3, and 4 μm were recorded as groups "D2," "D3," and "D4." It can be seen that the "D2" group consistently showed the largest bacterial proliferation area at different times, while the bacterial proliferation of the "D3" and "D4" groups was significantly inhibited (Figure 4c and d). In addition, we found a strong link between the magnitude of the parameter and the inhibitory capacity. The "D3" group, which had an area of bacterial proliferation of less than 50%, was significantly better than the other two groups after 24 h. This indicates that the magnitude of this parameter is not a determining factor of antimicrobial performance of the microstructures, as testing needs to be performed to identify the specific value of the parameter that can lead to the most significant antimicrobial performance. Taken together, our findings offer new ideas and methods for the study of antimicrobial mechanisms in microstructures.

4. Discussion

Bacteria have a profound impact on human existence, and their various roles affect our well-being and the environment.[34,35] These microscopic organisms play a crucial role in processes such as food spoilage, material

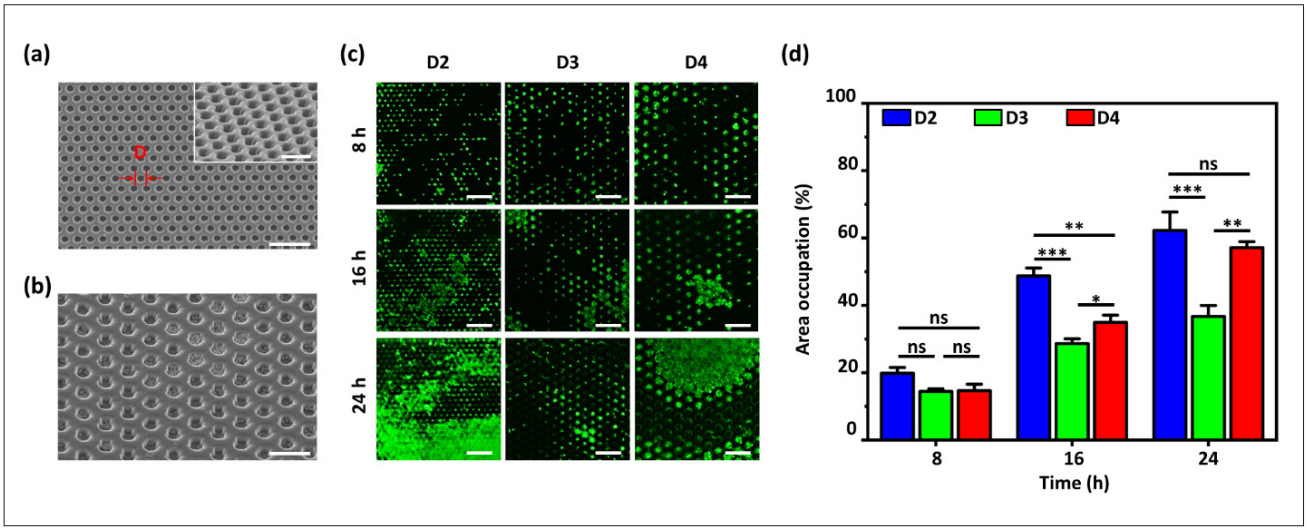

Figure 4. Precise modulation of microstructural morphology using two-photon polymerization 3D printing to study the key parameters affecting the bacterial inhibitory effect. The microstructural parameters: pore diameters (*D*) of 2, 3, and 4 μm. (a) 3D printing can precisely adjust the microstructure parameters. Scale bar: 20 and 10 μm (inset). (b) SEM image of bacterial proliferation on the surface of 3D-printed micropores for 24 h. Scale bar: 10 μm. (c) Proliferation of bacteria (green fluorescence-labeled) on the printed microporous structures with different parameters for 24 h. Scale bar: 30 μm. (d) The total area of the substrate occupied by the proliferating bacteria on the microporous structures with different parameters for 24 h. Data are expressed as mean ± SD. $n = 3$; one-way ANOVA; ns, no significance; *$p < 0.05$; **$p < 0.01$; ***$p < 0.001$. Abbreviation: SEM, scanning electron microscopy.

corrosion, immunity and environmental sustainability, and contributing to a range of diseases.[36–40] Several studies have found that some plant and animal surfaces have inherent antimicrobial capacity, due to the micro- and nano-structures on their surfaces.[41,42] In order to further explore the key factors and mechanisms of microstructure-induced antimicrobial effects, a processing technology that can precisely fabricate specific surface microstructures and accurately control the microstructural parameters is urgently required.

3D printing has emerged as a versatile and favorable platform for manufacturing a wide range of products with elaborate structures.[43,44] Two-photon polymerization 3D printing has been demonstrated to have many advantages in the precise printing of microstructures on a variety of surfaces as well as in the regulation of microstructural morphology, such as mild printing conditions, applicability to a wide range of material surfaces, and precise control of morphology parameters. The strategy of replicating bionic inhibitory microstructures on the surface of objects based on two-photon polymerization 3D printing shows great promise for application.[32,45]

It is now generally accepted that the mechanism of microstructure inhibition is primarily the stretching of the membrane region suspended between the nanocolumns as the bacterial cell encounters the surface of the column. Once the membrane is stretched enough, it will lead to rupture and eventually cell death.[46–48] It is certain that chemical inhibition is not involved in this inhibitory process. Bandara et al.[49] suggested that membrane damage to bacteria is achieved through strong adhesion between the nanopillar and the bacterial extracellular polysaccharide substance (EPS) layer. However, Linklater et al.[50] found that EPS did not play a role in the mechanical bactericidal action on the surface of the nanopillar by labeling the companion bean globulin using a label-tracking method. They also obtained black silicon surfaces with different morphologies and heights of microstructures by plasma etching silicon wafers[51] and found that the different surfaces of microstructures exhibited similar killing efficiencies against both *Pseudomonas aeruginosa* and *S. aureus* cells. However, limited by the etching technique, they could not precisely regulate other parameters of the nanopillars such as length, width, and spacing. This problem can be easily resolved by the two-photon polymerization 3D printing technique. Our study highlights the potential of two-photon polymerization 3D printing technology as an advanced fabrication technique for developing bacteriostatic micro-nano structures. By enabling precise control over microstructural parameters, two-photon polymerization 3D printing provides a powerful tool for systematically investigating the bacteriostatic mechanisms of bioinspired surfaces.

In this study, we simplified the microstructure that simulates shark skin. The simplified microstructure has the following advantages: first, the simplified structure inherits

the core features of the shark skin structure; second, the simplified structure is very regular, with three parameters that can be finely adjusted, including the width, height, and spacing of the rectangular columns, which facilitates the subsequent exploration of the mechanism; third, the simplified structure is relatively simple and intuitive, which is conducive to the generalization, extension, and improvement of the model as a research model; finally, the simplified structure is convenient for fabrication, reducing the cost and time of fabrication. Notably, the simplified microstructures had significant bacterial inhibitory property compared to the simulated structures. Our subsequent studies confirmed the parametric sensitivity of the inhibitory capacity of simplified microstructures. Previous studies, such as the one described above, have found that microstructures can achieve bacterial inhibition by disrupting the cell membranes of bacteria through stretching or cutting.[52] However, this phenomenon was not detected in our experiments using SEM images. In addition, the size change of the micron-scale structures had a negligible effect on the hydrophobicity of the microstructures.[52] The parametric sensitivity of the bacterial inhibitory ability is likely attributed to the following two factors: (i) the spatial restriction effect of the microstructure on the bacteria, and (ii) the effect of microstructure-bacteria contact mode on bacterial proliferation. This also explains the significantly enhanced inhibitory ability of the simplified microstructures, because they are far less smooth and continuous than the simulated ones, and the spatial restriction ability of the spaces between the rectangular columns is stronger than those of the simulated ones. Subsequently, we switched to a microporous structure and adopted an incremental diameter parameter design. The microporous structure is a model of a single parameter controlling the role of spatial restriction compared to the simplified structure of shark skin. From the results, the inhibitory ability of the microporous structure shows similar parametric sensitivity, and the effect of the parameter is dual. Therefore, we recommend enhancing the bacterial inhibitory capacity of both models by adjusting bacteria's spatial restriction and mode of contact with the microstructures.

The findings suggest that certain specialized microstructures exhibit a bacteriostatic effect, which becomes significant only when specific geometric parameters are met. One major limitation of the present study is that the fully delineated mechanism of bacterial inhibition remains uncovered, however, capitalizing on the advantages of two-photon polymerization 3D printing, such as high accuracy, efficiency, simplicity, and low cost, future studies can attempt on large-scale exploration of the mechanism, while expanding the parameter range and strain types. Moreover, the characteristics of microstructures such as morphology, parameters, and the corresponding bacterial inhibitory effect are easy to quantify. The data gathered can then be used to construct independent databases, as well as simulation models equipped with the excellent data processing capability of artificial intelligence, which provides a powerful tool for the screening of microstructures in terms of their morphology, parameters, and mechanism delineation. Taken together, the current research not only deepens our understanding of bacteriostatic mechanisms in micro-nanostructures but also paves the way for the development of next-generation bacteriostatic surfaces with applications in biomedical devices, implants, and healthcare/industrial products.[53–55]

5. Conclusion

In this paper, we demonstrate that parameter and morphology variations affect the physical inhibition of microstructures formed on the surface of an object using two-photon polymerization 3D printing technology. First, the simplified shark skin structures were able to inhibit the proliferation of more than 90% of *S. mutans* within 8 h and retained the same inhibitory effect at more than 70% after 24 h. Second, the height of the nanopillar had the greatest effect on the inhibitory ability of the microstructure against *S. mutans* compared to the spacing and width. This effect was also observed in other microstructures. In conclusion, we propose a novel strategy for exploring the mechanism of bacterial inhibition, i.e., to utilize the high-resolution and precise morphology control capability of two-photon 3D printing technology to precisely control the morphology of microstructures, so as to understand the underlying mechanism of bacterial inhibitory ability and the key influencing factors. This strategy is expected to fill the gap in the mechanism of physical bacterial inhibition, thereby improving the bacterial inhibitory effect and accelerating the application of this technology in industry, medicine, and daily life.

Acknowledgments

None.

Funding

This study was supported by Postdoctoral Science Foundation of China (2018M630883 and 2019T120688), Hubei Province Chinese Medicine Research Project (ZY2023Q015), Natural Science Foundation of Hubei Province (2023AFB665), Central Universities (Wuhan University) Clinical Medicine + X (2042024YXB017), the Medical Young Talents Program of Hubei Province, and Wuhan Young Medical Talents Training Project to L.-L. Bu,

Natural Science Foundation of China (61904057), Natural Science Foundation of Hubei Province (2018CFB124), and Research Programs of Science and Technology, Department of Education of Hubei Province (B2023256) to B. Cai, and International Orthodontics Foundation Young Research Grants Award (IOF2024Y11) to F.-Y. Huo.

Conflict of interest

The authors declare they have no competing interests.

Author contributions

Conceptualization: Fang-Yi Huo, Wentao Zhu, Kan Zhou, Enduo Zhou, Lei-Ming Cao, Qian Zhu, Hong He
Funding acquisition: Hong He
Investigation: Fang-Yi Huo, Wentao Zhu, Kan Zhou
Methodology: Fang-Yi Huo, Wentao Zhu, Kan Zhou, Enduo Zhou, Lei-Ming Cao, Qian Zhu
Project administration: Bo Cai, Lin-Lin Bu, Hong He
Supervision: Bo Cai, Lin-Lin Bu, Hong He
Visualization: Fang-Yi Huo
Writing–original draft: Fang-Yi Huo, Wentao Zhu, Kan Zhou, Enduo Zhou, Lei-Ming Cao, Qian Zhu
Writing–review & editing: All authors
All authors have reviewed and approved the final version of this manuscript for publication.

Ethics approval and consent to participate

Not applicable.

Consent for publication

Not applicable.

Availability of data

Data are available from the corresponding author upon reasonable request.

References

1. Otto M. Physical stress and bacterial colonization. *FEMS Microbiol Rev*. 2014;38(6):1250-1270. doi: 10.1111/1574-6976.12088
2. Byrd AL, Belkaid Y, Segre JA. The human skin microbiome. *Nat Rev Microbiol*. 2018;16(3):143-155. doi: 10.1038/nrmicro.2017.157
3. Muhammad MH, Idris AL, Fan X, et al. Beyond risk: bacterial biofilms and their regulating approaches. *Front Microbiol*. 2020;11:928. doi: 10.3389/fmicb.2020.00928
4. Nobbs AH, Lamont RJ, Jenkinson HF. Streptococcus adherence and colonization. *Microbiol Mol Biol Rev*. 2009;73(3):407-450. doi: 10.1128/mmbr.00014-09
5. Akcalı A, Lang NP. Dental calculus: the calcified biofilm and its role in disease development. *Periodontol 2000*. 2018;76(1):109-115. doi: 10.1111/prd.12151
6. Karygianni L, Ren Z, Koo H, Thurnheer T. Biofilm matrixome: extracellular components in structured microbial communities. *Trends Microbiol*. 2020;28(8):668-681. doi: 10.1016/j.tim.2020.03.016
7. Arciola CR, Campoccia D, Montanaro L. Implant infections: adhesion, biofilm formation and immune evasion. *Nat Rev Microbiol*. 2018;16(7):397-409. doi: 10.1038/s41579-018-0019-y
8. Sharma D, Misba L, Khan AU. Antibiotics versus biofilm: an emerging battleground in microbial communities. *Antimicrob Resist Infect Control*. 2019;8:76. doi: 10.1186/s13756-019-0533-3
9. Roy R, Tiwari M, Donelli G, Tiwari V. Strategies for combating bacterial biofilms: a focus on anti-biofilm agents and their mechanisms of action. *Virulence*. 2018; 9(1):522-554. doi: 10.1080/21505594.2017.1313372
10. Wu H, Moser C, Wang HZ, Høiby N, Song ZJ. Strategies for combating bacterial biofilm infections. *Int J Oral Sci*. 2015;7(1):1-7. doi: 10.1038/ijos.2014.65
11. Nwabuife JC, Omolo CA, Govender T. Nano delivery systems to the rescue of ciprofloxacin against resistant bacteria "E. coli; P. aeruginosa; Saureus; and MRSA" and their infections. *J Control Release*. 2022;349:338-353. doi: 10.1016/j.jconrel.2022.07.003
12. Fu X, Rehman U, Wei L, et al. Silver-dendrimer nanocomposite as emerging therapeutics in anti-bacteria and beyond. *Drug Resist Updat*. 2023;68:100935. doi: 10.1016/j.drup.2023.100935
13. Kalghatgi S, Spina CS, Costello JC, et al. Bactericidal antibiotics induce mitochondrial dysfunction and oxidative damage in Mammalian cells. *Sci Transl Med*. 2013;5(192):192ra85. doi: 10.1126/scitranslmed.3006055
14. Jaggessar A, Shahali H, Mathew A, Yarlagadda P. Bio-mimicking nano and micro-structured surface fabrication for antibacterial properties in medical implants. *J Nanobiotechnology*. 2017;15(1):64. doi: 10.1186/s12951-017-0306-1
15. Shahali H, Hasan J, Cheng HH, Ramarishna S, Yarlagadda PK. A systematic approach towards biomimicry of nanopatterned cicada wings on titanium using electron beam lithography. *Nanotechnology*. 2021;32(6):065301. doi: 10.1088/1361-6528/abbeaa
16. Xu M, Wang X, Wang B, et al. Carbonized lotus leaf/ZnO/Au for enhanced synergistic mechanical and photocatalytic

bactericidal activity under visible light irradiation. *Colloids Surf B Biointerfaces*. 2022;215:112468.
doi: 10.1016/j.colsurfb.2022.112468

17. Satheesh S, Ba-akdah MA, Al-Sofyani AA. Natural antifouling compound production by microbes associated with marine macroorganisms — a review. *Electron J Biotechnol*. 2016;21:26-35.
doi: 10.1016/j.ejbt.2016.02.002

18. Ge X, Ren C, Ding Y, et al. Micro/nano-structured TiO(2) surface with dual-functional antibacterial effects for biomedical applications. *Bioact Mater*. 2019;4:346-357.
doi: 10.1016/j.bioactmat.2019.10.006

19. Wang S, Deng Y, Yang L, Shi X, Yang W, Chen ZG. Enhanced antibacterial property and osteo-differentiation activity on plasma treated porous polyetheretherketone with hierarchical micro/nano-topography. *J Biomater Sci Polym Ed*. 2018;29(5):520-542.
doi: 10.1080/09205063.2018.1425181

20. Gao A, Yan Y, Li T, Liu F. Biomimetic urchin-like surface based on poly (lactic acid) membrane for robust anti-wetting and anti-bacteria properties. *Mater Lett*. 2019;237:240-244.
doi: 10.1016/j.matlet.2018.11.063

21. Li Y-N, Zhao Y, Liu J-J. Precisely engineered bionic Cu-doped titanium dioxide nanoarrays/fluorine-doped tin oxide with excellent antibacterial and antifouling properties. *Tungsten*. 2024;6(3):522-528.
doi: 10.1007/s42864-023-00255-9

22. Zhang Y, Zhao W, Chen Z, et al. Influence of biomimetic boundary structure on the antifouling performances of siloxane modified resin coatings. *Colloids Surf A: Physicochem Eng Aspects*. 2017;528:57-64.
doi: 10.1016/j.colsurfa.2017.05.044

23. Liu M, Wang S, Wei Z, Song Y, Jiang L. Bioinspired design of a superoleophobic and low adhesive water/solid interface. *Adv Mater*. 2009;21(6):665-669.
doi: 10.1002/adma.200801782

24. Cormican CM, Bektaş S, Martin-Martinez FJ, Alexander S. Emerging trends in bioinspired superhydrophobic and superoleophobic sustainable surfaces. *Adv Mater*. 2025;37(12):2415961.
doi: 10.1002/adma.202415961

25. Xu Y, Luan X, He P, et al. Fabrication and functional regulation of biomimetic interfaces and their antifouling and antibacterial applications: a review. *Small*. 2024; 20(21):e2308091.
doi: 10.1002/smll.202308091

26. Shao Z, Shen R, Gui Z, et al. Ethyl cellulose/gelatin/β-cyclodextrin/curcumin nanofibrous membrane with antibacterial and formaldehyde adsorbable capabilities for lightweight and high-performance air filtration. *Int J Biol Macromol*. 2024;254(Pt 2):127862.
doi: 10.1016/j.ijbiomac.2023.127862

27. Wu W, Han C, Liang R, et al. Fabrication and performance of graphene flexible pressure sensor with micro/nano structure. *Sensors (Basel)*. 2021;21(21):7022.
doi: 10.3390/s21217022

28. Gao Y, Ding Q, Li W, Gu R, Zhang P, Zhang L. Role and mechanism of a micro-/nano-structured porous zirconia surface in regulating the biological behavior of bone marrow mesenchymal stem cells. *ACS Appl Mater Interfaces*. 2023;15(11):14019-14032.
doi: 10.1021/acsami.2c22736

29. Chen Y, Wang C, Zhang Z, et al. 3D-printed piezocatalytic hydrogels for effective antibacterial treatment of infected wounds. *Int J Biol Macromol*. 2024;268(Pt 2):131637.
doi: 10.1016/j.ijbiomac.2024.131637

30. Jing X, Fu H, Yu B, Sun M, Wang L. Two-photon polymerization for 3D biomedical scaffolds: Overview and updates. *Front Bioeng Biotechnol*. 2022;10:994355.
doi: 10.3389/fbioe.2022.994355

31. Pao YH, Rentzepis PM. Laser-induced production of free radicals in organic compounds. *Appl Phys Lett*. 1965;6(5):93-95.
doi: 10.1063/1.1754182

32. Zhou X, Liu X, Gu Z. Photoresist development for 3D printing of conductive microstructures via two-photon polymerization. *Adv Mater*. 2024;36(48):2409326.
doi: 10.1002/adma.202409326

33. O'Halloran S, Pandit A, Heise A, Kellett A. Two-photon polymerization: fundamentals, materials, and chemical modification strategies. *Adv Sci (Weinh)*. 2023;10(7):e2204072.
doi: 10.1002/advs.202204072

34. Sanders ME, Akkermans LM, Haller D, et al. Safety assessment of probiotics for human use. *Gut Microbes*. 2010;1(3):164-185.
doi: 10.4161/gmic.1.3.12127

35. Chowdhury MAH, Ashrafudoulla M, Mevo SIU, Mizan MFR, Park SH, Ha SD. Current and future interventions for improving poultry health and poultry food safety and security: a comprehensive review. *Compr Rev Food Sci Food Saf*. 2023;22(3):1555-1596.
doi: 10.1111/1541-4337.13121

36. Chitrakar B, Zhang M, Adhikari B. Dehydrated foods: are they microbiologically safe? *Crit Rev Food Sci Nutr*. 2019;59(17):2734-2745.
doi: 10.1080/10408398.2018.1466265

37. Xu D, Gu T, Lovley DR. Microbially mediated metal corrosion. *Nat Rev Microbiol*. 2023;21(11):705-718.
doi: 10.1038/s41579-023-00920-3

38. Battaglia TW, Mimpen IL, Traets JJH, et al. A pan-cancer analysis of the microbiome in metastatic cancer. *Cell*. 2024;187(9):2324-2335.e19.
doi: 10.1016/j.cell.2024.03.021

39. Yong J, Chew KW, Khoo KS, Show PL, Chang JS. Prospects and development of algal-bacterial biotechnology in environmental management and protection. *Biotechnol Adv*. 2021;47:107684. doi: 10.1016/j.biotechadv.2020.107684

40. Roager HM, Licht TR. Microbial tryptophan catabolites in health and disease. *Nat Commun*. 2018;9(1):3294. doi: 10.1038/s41467-018-05470-4

41. Skoulas E, Manousaki A, Fotakis C, Stratakis E. Biomimetic surface structuring using cylindrical vector femtosecond laser beams. *Sci Rep*. 2017;7:45114. doi: 10.1038/srep45114

42. Li Y, Zhang LY, Zhang C, Zhang ZR, Liu L. Bioinspired antifouling Fe-based amorphous coating via killing-resisting dual surface modifications. *Sci Rep*. 2022;12(1):819. doi: 10.1038/s41598-021-04746-y

43. Zhu W, Ma X, Gou M, Mei D, Zhang K, Chen S. 3D printing of functional biomaterials for tissue engineering. *Curr Opin Biotechnol*. 2016;40:103-112. doi: 10.1016/j.copbio.2016.03.014

44. Su R, Chen J, Zhang X, et al. 3D-printed micro/nano-scaled mechanical metamaterials: fundamentals, technologies, progress, applications, and challenges. *Small*. 2023;19(29):e2206391. doi: 10.1002/smll.202206391

45. Zhang Y, Su Y, Zhao Y, Wang Z, Wang C. Two-photon 3D printing in metal-organic framework single crystals. *Small*. 2022;18(18):e2200514. doi: 10.1002/smll.202200514

46. Ivanova EP, Hasan J, Webb HK, et al. Bactericidal activity of black silicon. *Nat Commun*. 2013;4:2838. doi: 10.1038/ncomms3838

47. Ivanova EP, Hasan J, Webb HK, et al. Natural bactericidal surfaces: mechanical rupture of *Pseudomonas aeruginosa* cells by Cicada wings. *Small*. 2012;8(16):2489-2494. doi: 10.1002/smll.201200528

48. Linklater DP, Nguyen HKD, Bhadra CM, Juodkazis S, Ivanova EP. Influence of nanoscale topology on bactericidal efficiency of black silicon surfaces. *Nanotechnology*. 2017;28(24):245301. doi: 10.1088/1361-6528/aa700e

49. Bandara CD, Singh S, Afara IO, et al. Bactericidal effects of natural nanotopography of dragonfly wing on Escherichia coli. *ACS Appl Mater Interfaces*. 2017;9(8):6746-6760. doi: 10.1021/acsami.6b13666

50. Linklater DP, Juodkazis S, Rubanov S, Ivanova EP. Comment on "Bactericidal Effects of Natural Nanotopography of Dragonfly Wing on Escherichia coli". *ACS Appl Mater Interfaces*. 2017;9(35):29387-29393. doi: 10.1021/acsami.7b05707

51. Wang X, Bhadra CM, Yen Dang TH, et al. A bactericidal microfluidic device constructed using nano-textured black silicon. *RSC Adv*. 2016;6(31):26300. doi: 10.1039/C6RA03864F

52. Zhu WT, Huo FY, Cao LM, et al. Two-photon polymerization 3D printing of biomimetic microstructures for functionalizing surfaces to inhibit bacterial growth. *Chem Eng J*. 2025;511:161907. doi: 10.1016/j.cej.2025.161907

53. Li B, Tan H, Anastasova S, Power M, Seichepine F, Yang GZ. A bio-inspired 3D micro-structure for graphene-based bacteria sensing. *Biosens Bioelectron*. 2019;123:77-84. doi: 10.1016/j.bios.2018.09.087

54. Akbari E, Buntat Z, Afroozeh A, Zeinalinezhad A, Nikoukar A. Escherichia coli bacteria detection by using graphene-based biosensor. *IET Nanobiotechnol*. 2015;9(5):273-279. doi: 10.1049/iet-nbt.2015.0010

55. Krishnamurthi VR, Harris N, Rogers A, Zou M, Wang Y. Interactions of E. coli with cylindrical micro-pillars of different geometric modifications. *Colloids Surf B Biointerfaces*. 2022;209(Pt 2):112190. doi: 10.1016/j.colsurfb.2021.112190